A Novel Forest Dynamic Growth Visualization Method by Incorporating Spatial Structural Parameters Based on Convolutional Neural Network

Linlong Wang, *Student Member, IEEE*, Huaiqing Zhang, *Senior Member, IEEE*, Kexin Lei, Tingdong Yang, Jing Zhang, Zeyu Cui, Rurao Fu, *Student Member, IEEE*, Hongyan Yu, Baowei Zhao, and Xianyin Wang

***Abstract*—Current visual methods of forest dynamic growth mostly focus on the plot or stand level, which cannot express the morphological and structural characteristics of individual trees, as well as their statistical linkages, and causes each tree in the stand to grow at the same rate. In addition, these visual growth models still have some space for improvement in terms of prediction accuracy and multirelational data mining. In this article, uneven-aged Chinese fir (*Cunninghamia lanceolata*) plantations were chosen as our study subject and proposed a novel method of forest dynamic growth visualization modeling by incorporating spatial structure parameters and using convolutional neural network technique (FDGVM-CNN-SSP) to explore the effect of spatial structure on the morphological growth and to develop a prediction growth model of Chinese fir plantations by introducing a convolutional neural network (CNN) model. The results show that: first, spatial structural parameters C and U have a certain contribution to the forest growth, and C and U can explain 21.5%, 15.2%, and 9.3% of the variance in DBH, H, and CW growth models, respectively; second, CNN model outperformed machine learning algorithms SVR, MARS, Cubist, RF, and XGBoost in terms of prediction performance; third, based on FDGVM-CNN-SSP, we simulated Chinese fir plantations at individual tree level and stand level from 2018 to 2022 and found that DBH and H's fitting performance in measured and predicted data was highly consistent with R^2 and root-mean-square error (RMSE) of 86.8%, 2.06 cm in DBH and 79.2%, 1.11 m in H, but CW's R^2 and RMSE of 72.2%, 0.65 m caused crowding (C) inconsistency.**

***Index Terms*—Convolutional neural network (CNN), forest growth model (FGM), spatial structure, three-dimensional (3-D) visualization.**

Manuscript received 6 October 2023; revised 16 November 2023; accepted 8 December 2023. Date of publication 13 December 2023; date of current version 24 January 2024. This work was supported in part by the National Key R&D Program of China under Grant 2022YFE0128100 and in part by the National Natural Science Foundation of China under Grant 32271877 and Grant 32071681. *(Corresponding author: Huaiqing Zhang.)*

Linlong Wang is with the Institute of Forest Resource Information Techniques and Research Institute of Forest Policy and Information, Chinese Academy of Forestry, Beijing 100091, China (e-mail: wangll@ifrit.ac.cn).

Huaiqing Zhang, Kexin Lei, Tingdong Yang, Jing Zhang, Zeyu Cui, and Rurao Fu are with the Institute of Forest Resource Information Techniques, Chinese Academy of Forestry, Beijing 100091, China (e-mail: zhang@ifrit.ac.cn; leikx@ifrit.ac.cn; yangtd@ifrit.ac.cn; zhangjing@ifrit.ac.cn; cuizeyu@ifrit.ac.cn; frao.20201@outlook.com).

Hongyan Yu, Baowei Zhao, and Xianyin Wang are with the Qinghai Service Support Center, Qilian Mountain National Park, Qinghai 810001, China (e-mail: yuhy502@yeah.net; qlsdsjzx@163.com; wxying_1219@163.com).

Digital Object Identifier 10.1109/JSTARS.2023.3342445

I. Introduction

THREE-DIMENSIONAL (3-D) forest dynamic growth visual method plays an important role in forest management simulation and health monitoring, which helps forest managers intuitively perceive tree growth states and predict future forest resource conditions for forest planning and decision-making [1], [2], [3], [4]. As the basic component of virtual forest stand dynamic growth simulation, forest growth model (FGM) allows the virtual forest stand to grow like a real forest along the natural succession [2], [5]. Current virtual forest growth research primarily focuses on stand or diameter class growth models [6], [7], [8], [9], which fail to account for morphological and structural changes at the individual tree level under varied growth conditions. Therefore, it is necessary to construct an FGM at the individual tree level to capture the dynamic morphological characteristics of individual trees and to provide information for users in a virtual forest platform.

Existing individual tree growth models usually have been developed as a function of tree size, competition, site conditions, and climate factors [10], [11], [12], [13], [14]. For example, diameter at breast height (DBH), height-diameter ratio, and dominant height [15], [16], [17] have a great contribution on crown width increment; tree height increment may be affected by factors such as precipitation, winds, nutrients and sunshine duration [18], [19], [20], and temperature [21], [22]. Diameter growth with spatially competition indices predicts growth better than nonspatial ones [23], [24]. However, in a highly structurally forest environment, the impact of individual trees' spatial structure at a small scale on the forest stand growth has been ignored. Current research on the relationship between spatial structure parameters and tree growth characteristics mainly focuses on the competition index (CI) [25], [26], [27], [28], which can only describe the effect of overall or unilateral structure of the reference tree on tree growth traits and the effect of size differentiation, tree distribution, tree species segregation, and the degree of crowding remains unknown.

Individual growth models in forestry mostly employed statistical models such as linear and nonlinear regression models with or without random effects [29], [30], [31], [32]. These statistical models are commonly implemented under particular statistical assumptions, such as the plot data need to be independent, homoscedastic, and normally distributed [15], [16], [33].

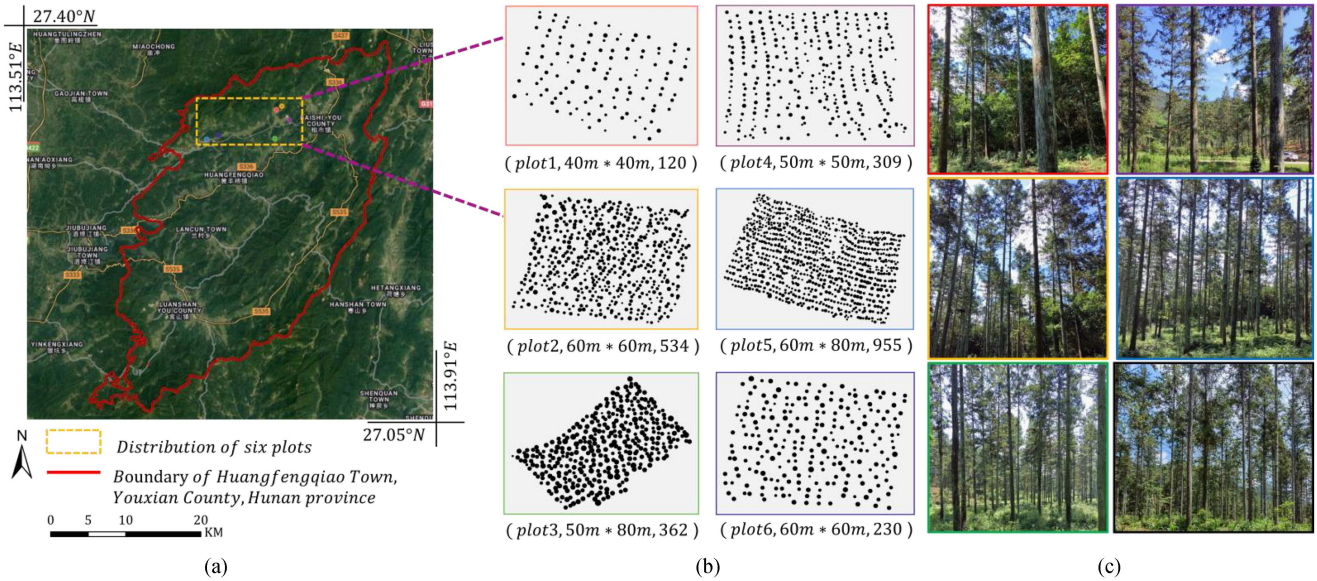

Fig. 1. General situations of the study area. (a) Location of the study area and the six experimental sites within Huangfengqiao Town, Youxian County, Hunan Province, China. (b) DBH size, geographical distribution of each tree in the six experimental sites; different sizes of circles represent DBH size; the plot number, plot size, and number of trees were in order included in round bracket. (c) Photographs show the stand characteristics of the six experimental sites.

Nevertheless, these assumptions are difficult to meet for forest growth data and time-consuming for data preprocessing [34]. In addition, choosing a mathematical equation and achieving convergence are difficult when modeling individual tree growth with multiple variables [15], [16], [33]. However, machine learning techniques are becoming more popular in forestry because they can predict tree growth better without making assumptions about input data distribution. For example, Hamidi et al. [35] show that machine learning SVR outperforms regression analysis by including numerous variables when predicting nonlinear systems and complex linkages. Ou et al. [36] and Cheng et al. [37] argue that RF, MARS, and Cubist models are effective and powerful modeling methods for predicting the growth of individual tree diameter. Recently, some researchers have found that deep learning models are preferred by scientists and researchers because they provide better predictions compared to traditional machine learning methods [38]. For example, Bueno et al. [39] support that ANN predicted crown diameter more accurately than machine learning methods RF, SVR, and REG. Qin et al. [40] argue that the DNN model performs better in predicting crown width when all input variables are included.

Therefore, in order to accurately model 3-D forest stand dynamic growth in a spatially diverse and heterogeneous environment, we will choose an uneven-aged Chinese fir (*Cunninghamia lanceolata*) with 13–28 years old as our subject, which was a typical forest stand in a subtropical region of China. The following two aspects were explored in this study: 1) to develop the morphological characteristics (e.g., tree height, DBH, and crown width) growth model at the individual tree level with highly heterogeneous spatial structures by introducing convolutional neural network (CNN) technique and 2) to optimize a visual method of forest growth at stand level by incorporating individual parameters of spatial structure parameters based on a small-scale forest stand in order to achieve visual simulation of forest growth at both individual tree level and stand level under heterogeneous forest conditions.

II. Material and Methods

A. Study Area and Data Acquisition

1) Study Area: The study area covers the uneven-aged Chinese fir plantation in Huangfengqiao Town, Youxian County, Hunan Province, southern China region (113°30′36″∼113°54′36″E, 27°03′∼27°24′N) (see Fig. 1). From 2012 to 2017, average temperatures in Youxian County ranged from 18.7 °C to 19.1 °C, with the minimum average temperatures ranging from 6.6 °C to 9.6 °C and the maximum temperature reaching 26.6 °C to 30.4 °C in the distribution zones of Chinese fir plantations used in the study. The total annual rainfall varies from 1312 to 1811 mm (with a disparate distribution of rainfall over a year), and relative humidity (RH) ranges from 70% to 77%. The climatic regime is a subtropical monsoon humid climate with a moderate, less rainy winter and a hot, rainy summer. The elevation of the study area varied from 270 to 320 m, whereas the slope ranged between 5° and 10°. The study area was a pure Chinese fir plantation that had been thinned for once or once more, resulting in the development of typical heterogeneous, uneven-aged, pure Chinese fir plantations within the study area.

2) Data Acquisition: The data were collected from six square sample plots with a range of stand ages, tree size, and percent density (see Fig. 1) from 2012 to 2017. The sample plot sizes in the study varied between 2250 and 4800 m^2. Azimuth angle, distance from plot center [for X and Y coordinates (m)], DBH, total height (H), average crown width at the base of the living crown (CW), crown base height (HB), crown length

(CL), crown ratio (CR), crown shape ratio (CSR), and crown fullness ratio (CFR) of each tree (totaling 11 154) in six sample plots were measured during 2012–2017 for all trees with a DBH of ≥5 cm, and their locations were recorded using a total station (TOPCON-GTS-602AF). In addition, annual increment of DBH (△DBH), annual increment of height (△H), and annual increment of crown width (△CW) of each tree (totaling 11 154) were measured during 2013–2017. The total number of tree size variables is 28. A detailed description of tree size is shown in the Appendix (see Fig. 11).

Competition indices are generally used as an explanatory variable in individual-tree growth and yield models as competition among trees strongly influences growth relationships. A total of 20 competition indices including nine distance-independent CI1–CI9 and 11 distance-dependent types CI10–CI20, and eight methods of determining competitors consisting of the crown overlap method (M1) [41], the fixed-radius method (M2, CZR0.4h) [42], the fixed-radius method (M3, $k = 2$) [42], the angle count sampling method (M4, BAF = 4) [43], the vertical search cone method (M5, apx in stem base of subject tree) [44], the vertical search cone method (M6, apx in crown base height of subject tree) [44], the nearest neighbor method (M7) [45], and Voronoi diagrams method (M8) [46], were selected based on detailed cultural heritage sorting and reading. The total number of competition indices is 139. The formula of CI1–CI20 competition indices is given in the Appendix (see Fig. 12).

Temperature and precipitation both have an impact on the physiological and growth processes of plant species [47], [48]. The climate data in Huangfengqiao National Forest Farm from 2012 to 2017 are obtained from the ClimateAP software, including 1) temperature related: mean annual temperature, mean warmest month temperature, mean coldest month temperature, extreme minimum temperature over 30 year average, extreme maximum temperature over 30 year average, degree days subzero (DD_0), degree days above 5 °C (DD5), degree days below 18 °C (DD_18), degree days above 18 °C (DD18); 2) precipitation related: continentality (TD), mean annual precipitation, mean spring precipitation, annual heat-moisture index, summer heat-moisture index, precipitation as snow, Hargreaves reference evaporation (Eref), Hargreaves climatic moisture deficit, mean annual RH; 3) illumination related: number of frost-free days, frost-free period, and mean annual solar radiation. The total number of climate factors is 21.

Soil conditions can significantly influence tree growth rate, with more nutrient-rich soils producing faster growth [30], [49]. The soil data in the six experimental sites are downloaded by Google Earth Engine and extracted from SoilGrids map, including bulk density of the fine earth fraction (Bdod, kg/dm³), cation exchange capacity of the soil (Cec, cmol(c)/kg), volumetric fraction of coarse fragments (>2 mm) (Cfvo, $cm^3/100cm^3$), total nitrogen (Nitrogen, g/kg), soil pH (phh2o, pH), proportion of sand particles (>0.05 mm) in the fine earth fraction (Sand, %), proportion of silt particles (≥0.002 mm and ≤0.05 mm) in the fine earth fraction (Silt, %), proportion of clay particles (<0.002 mm) in the fine earth fraction (Clay, %), soil organic carbon content in the fine earth fraction (Soc, g/kg), organic carbon density (Ocd, kg/m³), and organic carbon stocks (Ocs, kg/m^2). The total number of site factors is 11.

Forest structure is the driving force behind forest growth and biological processes, particularly in a diverse heterogeneous environment [50]. In order to express the spatial information at the individual tree level, we will adopt the quantitative analysis method of spatial structure based on the relationships of nearest neighbor trees, which can describe the spatial distribution pattern, species diversity, size diversity, crowding degree diversity by a set of structural stand parameters: Wi, Mi, Ci, Ui. Wi, Mi, Ci, Ui are calculated with the six plot field data according to Hui et al. [51]. For six plots consisting of a pure Chinese fir plantation, the value of Mi was set to 0 in our study. The total number of spatial structural parameters is 4.

3) Plot Characteristics: Descriptive statistics including mean, minimum, maximum, standard deviation, and coefficient variation of tree size components such as annual diameter increment (△DBH), annual height increment (△H), annual crown width increment (△CW), total height (H), DBH, crown width (CW), height to crown base (HCB), CR, basal area (BA), CL, CSR, and CFR, of spatial structural parameters such as tree distribution (Wi), tree species (Mi), tree size (Ui), tree crowding (Ci) in space, and of 20 competition indices (CI1–CI20) with M1 method are listed in Table I. This dataset was randomly partitioned into model training and validation datasets, consisting of 70% and 30% of the total datasets, respectively.

B. Construction of FGMs With SSP at Individual Tree Level

1) Determination of Growth Model Form: The growth dynamics of individual trees are commonly represented by mathematical models that incorporate several factors such as tree size, competition, site quality, and environmental variables [36]. Furthermore, some researchers have discovered that within a forest environment characterized by high heterogeneity, the spatial structure significantly influences the morphological features of individual trees [33]. Therefore, we added spatial structural variables into the model to explore the impact of single spatial structure variables or their interaction with other variables on tree growth. The model form was expressed as follows:

$$\Delta\ (\mathrm{DBH}, \mathrm{H}, \mathrm{CW}) = f\left(\mathrm{Size}, \mathrm{Competition}, \mathrm{Site}, \mathrm{Climate},\ \mathrm{Spatial\ Structure}\right).$$

2) Independent Variable Selection: Considering the simplicity and efficiency of the model, we will use the random forest (RF) for the selection of independent variables because it has high predictive accuracy, covers the effects of each predictor variable as well as multivariate interactions with other predictor variables [52], and is applicable even to high-dimensional problems with highly correlated variables. Two indices: % IncMSE and IncNodePurity were always selected as indicators of the variable importance of the independent variables involved. Given the issue of mismatch of % IncMSE and IncNodePurity, in our study, we will choose % IncMSE as an index for the importance ranking of these variables. To select the optimal number of variables for growth prediction of DBH, H, and CW, the rfcv

TABLE I
DESCRIPTIVE STATISTICS OF TREE SIZE, SPATIAL STRUCTURE, AND COMPETITION INDICES

Variables	Training datasets					Validation datasets				
	Min	Max	Mean	SD	CV%	Min	Max	Mean	SD	CV%
Tree Size Components:										
- △DBH (cm)	0.02	1.43	0.63	0.31	49.58	0.02	1.40	0.63	0.31	49.22
- △H (m)	0.02	1.50	0.71	0.49	69.21	0.02	1.49	0.76	0.52	68.83
- △CW (m)	0.05	1.20	0.29	0.25	86.50	0.05	1.31	0.28	0.24	87.21
- DBH (cm)	3.30	36.0	17.64	5.22	29.62	4.40	35.86	17.62	5.20	29.53
- H (m)	4.10	29.5	13.24	3.09	23.37	4.10	23.32	13.21	3.02	22.89
- CW (m)	0.50	12.4	3.47	0.91	26.36	0.85	11.9	3.46	0.89	25.90
- HCB (m)	0.20	18.4	7.66	2.40	31.33	0.00	17.5	7.66	2.36	30.89
- BA (m^2*10^{-2})	0.08	10.17	2.65	1.55	58.47	0.15	10.09	2.64	1.54	58.36
- CL (m)	0.10	21.0	5.58	2.16	38.85	0.36	16.36	5.55	2.15	38.76
- CR	0.01	1.15	0.49	0.23	47.14	0.04	1.15	0.48	0.23	47.02
- CSR	0.00	0.96	0.27	0.05	19.62	0.07	0.81	0.26	0.05	19.42
- CFR	0.00	30.0	0.71	0.50	70.56	0.18	6.7	0.71	0.36	51.60
Spatial Structure:										
- Distribution, Wi	0.00	1.00	0.4332	0.18	43.64	0.00	1.00	0.4309	0.18	43.04
- Mingling, Mi	——	——	——	——	——	——	——	——	——	——
- Crowding, Ci	0.00	1.00	0.8600	0.21	24.25	0.00	1.00	0.8579	0.20	24.39
- Dominance, Ui	0.00	1.00	0.4719	0.35	75.03	0.00	1.00	0.4740	0.35	74.06
Competition Indices:										
- CI1	0.00	44.46	18.24	9.48	52.04	0.00	44.11	18.28	9.38	51.30
- CI2 ($*10^{-4)}$	2.80	50.0	11.4	4.98	43.56	3.46	49.86	11.4	4.7	41.33
- CI3	0.02	0.15	0.06	0.02	31.04	0.02	0.14	0.06	0.02	31.00
- CI4	0.14	1.00	0.59	0.14	23.39	0.18	1.00	0.59	0.14	23.26
- CI5	0.06	3.38	1.00	0.42	41.78	0.10	3.34	0.99	0.42	42.06
- CI6	0.02	1.00	0.37	0.17	45.29	0.03	1.00	0.37	0.17	45.28
- CI7	0.52	63.91	4.61	2.85	61.34	0.77	38.13	4.58	2.58	56.38
- CI8	3.07	374.2	28.17	17.63	63.20	4.54	233.3	27.94	16.5	59.31
- CI9	0.00	1.09	0.30	0.24	82.47	0.00	1.08	0.29	0.24	83.62
- CI10	0.00	103.8	10.9	9.15	83.61	0.00	102.6	10.7	9.05	83.89
- CI11	0.00	11.6	1.54	0.87	53.38	0.00	5.94	1.51	0.82	55.03
- CI12	0.00	3.03	0.79	0.46	58.79	0.00	3.15	0.79	0.47	60.02
- CI13	0.00	6.25	0.87	0.63	72.59	0.00	5.02	0.87	0.64	72.89
- CI14	0.40	56.95	6.08	4.41	58.61	0.43	81.79	5.93	4.20	70.92
- CI15	0.00	29.81	2.06	1.39	67.62	0.00	24.21	2.02	1.28	63.63
- CI16	0.00	21.01	2.17	1.85	85.44	0.00	21.16	2.14	1.84	86.36
- CI17	0.00	0.27	0.06	0.05	90.69	0.00	0.27	0.06	0.05	92.53
- CI18	0.00	119.6	17.8	12.4	69.88	0.00	122.8	17.5	12.2	70.11
- CI19	0.00	0.10	0.02	0.02	94.83	0.00	0.11	0.02	0.02	98.81
- CI20	0.00	0.30	0.03	0.02	78.73	0.00	0.27	0.03	0.02	76.91

function in the randomForest package was used. This function compares the cross-validated prediction performance of models when the number of predictors is reduced [53]. Based on the recommendations of Carvajal et al. [54], the rfcv function was repeated 10 times, with 10-fold cross-validation, to determine the optimal number of variables.

3) Construction of FGMs: Because of their versatility in dealing with complex and numerous interacting variables, new modeling approaches such as machine learning and deep learning methods have recently gained popularity and interest [38], [39], [40]. The CNN [55], which is widely acknowledged as one of the most effective and regularly employed deep learning algorithms, has produced significant improvements in contemporary forestry research. As a result, in addition to the popular machine learning algorithms (e.g., SVR, MARS, Cubist, RF, XGBoost), CNN is used in our study to model forest growth. ΔDBH, ΔH, ΔCW were modeled as explanatory variables with these selected independent variables in Section II-B2 to examine the link between morphological features annual increment and variables of tree size, competition, site, climate, and spatial structure. For different scenarios, different models have different parameters and functions setting. As shown in Fig. 2, the datasets consisting of ΔDBH, ΔH, ΔCW, and selected independent variables were randomly partitioned into two parts: model training and validation datasets, which account for 70% and 30% of the total datasets, respectively. The datasets were under preprocessing of "center" and "scale," to ensure all data in the same dimension for analysis and comparison of different models. The method "cv" and "number = 10" mean the method of 10-fold cross-validation, which was used to reduce the dimension of the data and determine the best model for predicting the ΔDBH, ΔH, and ΔCW. Fig. 2 summarizes the workflow of growth model construction and detailed parameters setting for model training.

4) Comparison of Model Performance and Model Selection: 10-fold cross-validation resampling method was used to assess the prediction accuracy during the estimation of ΔDBH, ΔH, ΔCW. Three measures for model performance were computed

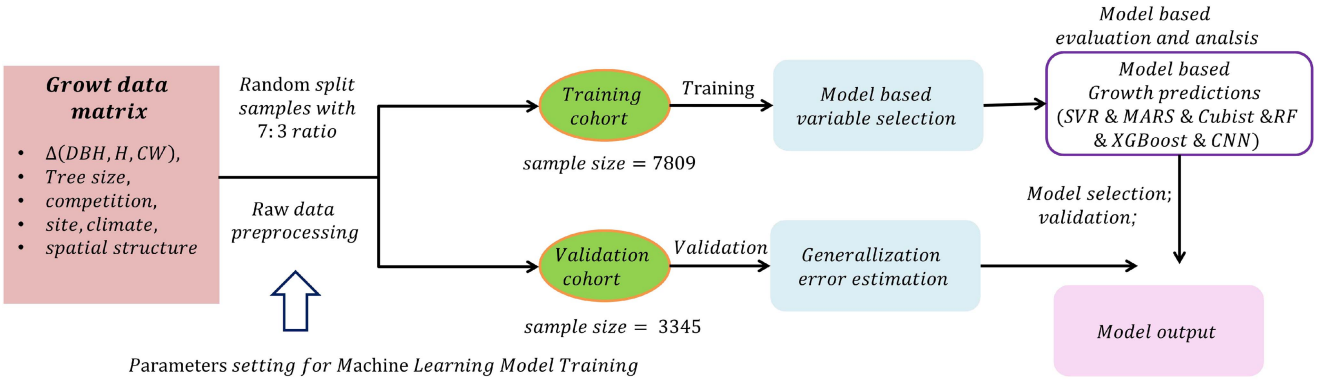

Parameters setting for Machine Learning Model Training

Model	DataPartition	Preprocessing	method	traincontrol	TuneGrid
SVR	training : validation=7:3	'center','scale'	svm	method='cv', number=10	C=seq(0, 1, by=0.5), sigma=0.1
MARS	training : validation=7:3	'center','scale'	earth	method='cv', number=10	nprune=c(1:112), degree=1
Cubist	training : validation=7:3	'center','scale'	cubist	method='cv', number=10	committees=c(1:100), neighbors=c(5,9)
RF	training : validation=7:3	'center','scale'	rf	method='cv', number=10	mtry=c(1:102), nTrees=1000
XGBoost	training : validation=7:3	'center','scale'	xgbTree	method='cv', number=10	eta = c(0.001, 0.005, 0.01, 0.02, 0.05, 0.1, 0.2, 0.3), max_depth = c(2, 4, 6, 8), subsample = c(0.5, 0.75, 1), gamma = c(1, 2, 3), min_child_weight = c(1, 2, 3)
CNN	training : validation=7:3	'center','scale'	cnn	method='cv', number=10	filters=64, kernel_size=2, activation='relu', optimizer='adam', epochs=50000, batch_size=16

Fig. 2. Workflow of grow model construction and parameters setting for model training.

for each fold: coefficient of determination (R^2), root-mean-square error (RMSE), and mean absolute errors (MAE). Then, the 10 resampled validation measurements of model performance were averaged as follows. It is desired that R^2 be close to 1 and RMSE, MAE values be low

$$R^2_{CV} = \frac{1}{k}\sum_{j=1}^{k}\left(R^2_j\right) = \frac{1}{k}\sum_{j=1}^{k}\left(1-\left[\frac{\sum_{i=1}^{n_j}\left(y_{ij}-\hat{y}_{ij}\right)^2}{\sum_{i=1}^{n_j}\left(y_{ij}-\bar{y}_j\right)^2}\right]\right) \quad (1)$$

$$RMSE_{CV} = \frac{1}{k}\sum_{j=1}^{k}\left(RMSE_j\right) = \frac{1}{k}\sum_{j=1}^{k}\left(\sqrt{\frac{\sum_{i=1}^{n_j}\left(y_{ij}-\hat{y}_{ij}\right)^2}{n_j}}\right) \quad (2)$$

$$MAE_{CV} = \frac{1}{k}\sum_{j=1}^{k}\left(MAE_j\right) = \frac{1}{k}\sum_{j=1}^{k}\left(\sqrt{\frac{\sum_{i=1}^{n_j}\left|y_{ij}-\hat{y}_{ij}\right|}{n_j}}\right) \quad (3)$$

where k is the number of fold, and $k = 10$ in our study; y_{ij} is the ith observed value of the jth fold; $\hat{y}_{ij}$ is the ith predicted values of the jth fold; $\bar{y}_j$ is the average of observed value of the jth fold; and n_j is the number of observations in jth fold. R^2_{CV}, $RMSE_{CV}$, MAE_{CV} refer separately to the coefficient of determination of cross-validation, RMSE of cross-validation, and MAE of cross-validation; R^2_j, $RMSE_j$, MAE_j are the R^2, *RMSE*, and *MAE* of the jth fold, respectively.

C. FDGVM-CNN-SSP

1) FDGVM-CNN-SSP at Tree and Stand Level: Forest dynamic growth visualization commonly employs a plot or stand growth model, resulting in identical tree growth increment that does not conform to forestry norms and principles [3]. FDGVM-CNN-SSP was a dynamic growth visualization method at tree level by incorporating spatial structural information and using a CNN model to analyze the growth changes of individual tree (see Fig. 3). It was a cumulative process of individual tree modeling based on morphological data at stand level (see Fig. 4), and it adds these constraints of tree size, competition, climate, site, and spatial structure in the tree growth process, which is very close to the real growth of trees, and can be used to highly complex and heterogeneous forest simulation. Essentially, FDGVM-CNN-SSP is a cycle process of updating and assembling individual tree models in the virtual forest stand over time.

2) Basic Components of FDGVM-CNN-SSP: Our approach to FDGVM-CNN-SSP can be divided into three parts: A1, A2, and A3. A1 is the process of tree in the plot coupling the individual tree's spatial structural parameters (e.g., Wi, Mi, Ui, Ci), which is better for expressing more of a tree's spatial structural information, not only morphological characteristics (see Fig. 3). The value of (Wi, Mi, Ui, Ci) was calculated according to the formula in A3.

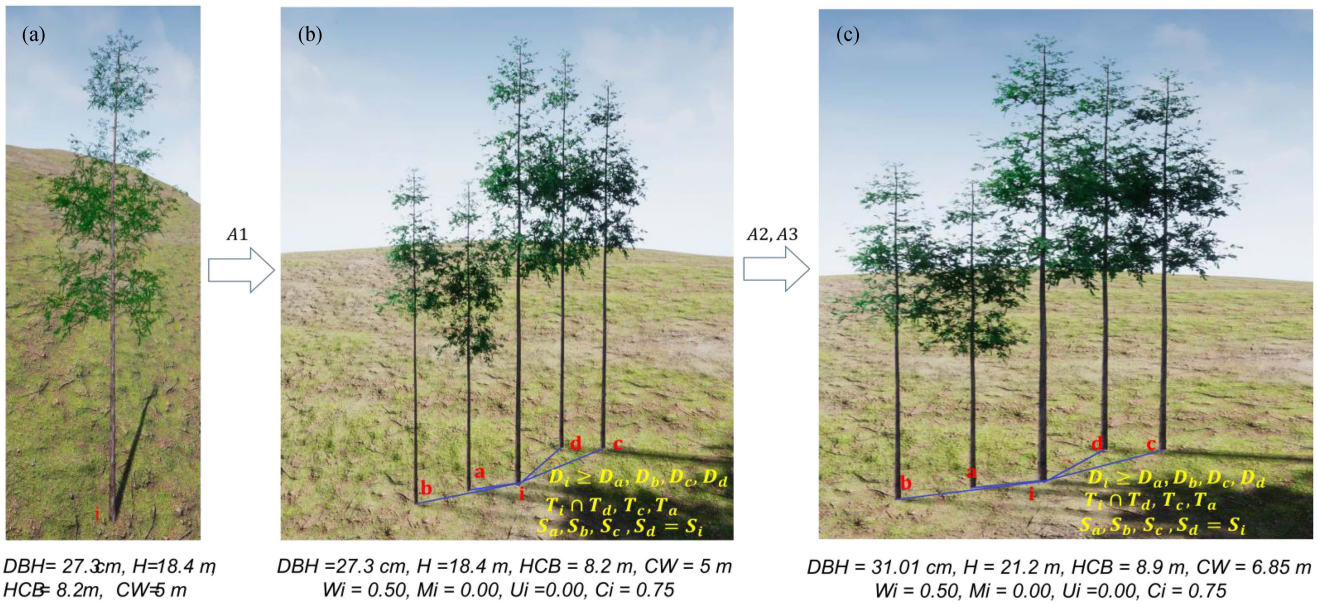

Fig. 3. FDGVM-CNN-SSP at tree level. Among (a), (b), and (c), i means the reference tree; a, b, c, d mean the four nearest tree of the reference tree i in the plot. The values of Wi, Mi, Ui, and Ci were 0.00, 0.25, 0.50, 0.75, and 1.00, respectively. A1 means the individual tree coupling SSP; A2 means forest dynamic growth model with CNN and SSP; A3 means update of New Tree_List_Attri table.

A2 is a forest dynamic growth model module based on CNN and SSP. The regression CNN model was used to estimate forest growth of DBH, H, and CW, as shown in Fig. 5. The input data including X_Size, X_Competition, X_Climate, X_Site, and X_SSP flow into a Conv1D network for feature extraction, followed by a flattened layer with making the multidimensional input into 1-D. Then, the input data are encoded by a feature vector (length = 832, 384, 192 in ΔDBH, ΔH, and ΔCW, respectively). Finally, we utilize two dense layers of 64, 32 neurons and further regress out the annual increment of DBH, H, and CW in the output layer. A rectified linear unit is applied after each convolutional layer and dense layer in the network, which performs the nonlinear transformation of the feature array generated by the convolution layer and dense layer. It is worth noting that, in order to balance the time-cost and model accuracy, the input variables for model of ΔDBH, ΔH, ΔCW in CNN are through feature selection by RF and matrix transformation in our method.

A3 is the update of Tree_List_Attri table module, which changes with the time. The initial Tree_List_Attri table contains the plot data collected by field observation, including the morphological trait (DBH, H, CW, HB) and spatial conditions (Ci, Mi, Wi, Ui) of each tree in the forest stand. The update process of Tree_List_Attri table is shown in Fig. 5. The value of (DBH, H, CW, HB) in the $(i+1)$_th year was updated by adding the value of △DBH, △H, △CW in the $(i+1)$_th year to the value of (DBH, H, CW, HB) in i_th year. The value of (Ci, Ui) was updated according to formula in A3. Finally, the 3-D forest scenes modeling was according to geographical coordinate (X,Y,Z) of each tree in plot and Tree_List_Attri table (initial year) or New Tree_List_Attri table (after initial year) based on UE4 engine.

TABLE II
SUMMARY OF INITIAL SETTINGS FOR △(DBH, H, CW) MODELS BY RF

Models	Dependent variable	Number of variables	nTrees	mtry	Time (min)
RF	△DBH	203	1000	3	7.91
	△H	203	1000	3	7.47
	△CW	203	1000	3	7.77

III. RESULT

A. Independent Variable Selection

The importance of top 14 predictive variables for a model of △(DBH, H, CW) is shown in Fig. 6, which showed the same %IncMSE trends by RF. For model of △(DBH, H, CW), the variable with the maximum IncMSE is CR, height (H), and height (H), respectively, which are suitable variable in tree size features, followed by uaCI, 1/D, CI1, C in △DBH model, uaCI, C, CR, 1/D in △H model, and C, CR, H_i, uaCI in △CW model, which all come from competition, tree size, and spatial structure. Although the specific selected variables differed, CR, uaCI, H, HB, C, and U were included in △(DBH, H, CW) models.

The number of selected features differed among △(DBH, H, CW) model. For a model of △DBH, the optimal number of variables was 14 based on the rfcv results (see Fig. 6). Therefore, the top 14 variables in the variable importance ranking were used in the final predictive model. For a model of △H, the optimal number of variables was seven, including H, uaCI, C, CR, 1/D, D_i, and CI18. For a model of △CW, the optimal number of variables was 4, including H, C, CR, and H_i. Table II summarizes the number of variables, ntree, mtry, and running time of three growth models by RF.

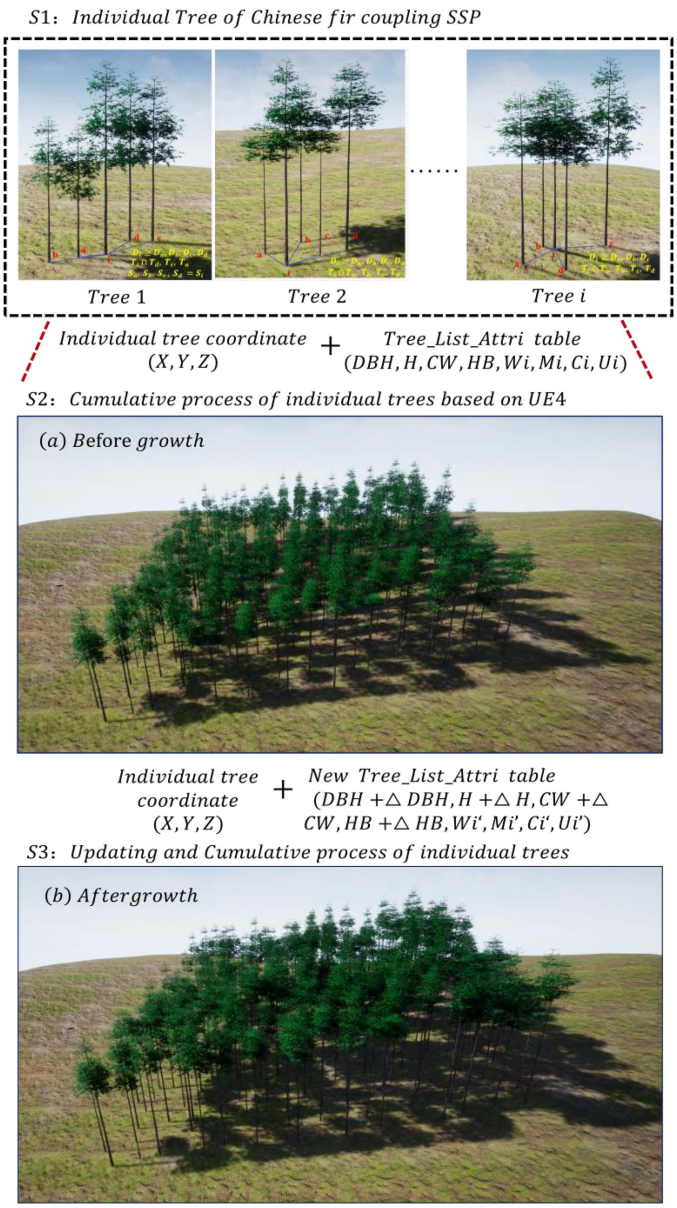

Fig. 4. FDGVM-CNN-SSP at stand level. Tree_List_Attri table and New Tree_List_Attri table were a DataTable in UE4 engine, which consists of the morphological data and spatial data for tree modeling, such as DBH, H, CW, HB, Wi, Mi, Ci, and Ui.

B. Estimation Models of Annual Increment of DBH, H, and CW

In the process of △(DBH, H, CW) model estimation, it is not only required to choose a good learning algorithm but also to find the proper parameters, which is generally referred to as "parameter tuning." Model performance can vary greatly based on the values used for the parameters. Therefore, parameter tuning was implemented and tested for the SVR, MARS, RF, Cubist, XGBoost, and CNN in our study. We will select RMSE as the evaluation indicator for tuning parameters. For SVR model, the final value of C, sigma is at (1, 0.1) △(DBH, CW) model, (0.80.1) in △H model; for Mars, the final value of Nprune, degree is at (22,1) in △DBH model, (13,1) in △H model, and (16,1) in △CW model; for Cubist, the final value of committee, neighbors is at (93,9) in △DBH model, (97,9) in △H model, (19) in △CW model; for RF, the final value of mtry, nTrees is at (4,1000) in △DBH model, (2,1000) in △H model, (1,1000) in △CW model; for CNN, the final value of epoch is at 5000 in △DBH model, 6000 in △H model, 6000 in △CW model by balancing the prediction accuracy and time-cost; for XGBoost, the final value of eta, max_depth, gamma,mini_child_weight, subsample is at (0.05, 8, 1, 2, 0.75) in △DBH model, (0.1, 8, 1, 2, 0.75) in △H model, and (0.2, 8, 1, 1, 1) in △CW mode. Fig. 7 summarizes the result of tuning parameters used for the model training.

C. Comparison of Model Performance and Model Selection

Table III shows the result of △(DBH, H, CW) model based on SVR, MARS, Cubist, RF, CNN, XGBoost regression models. Using R^2 and RMSE as the evaluation indicator, the CNN, XGBoost, RF, and Cubist models had a distinct advantage over MARS and SVR in predicting individual tree △(DBH, H, CW) growth models. In the training datasets, the CNN model ranked the highest in terms of performance (R^2:0.64; RMSE:0.19 cm) in △DBH, (R^2:0.52; RMSE:0.16 m) in △H, (R^2:0.48; RMSE:0.18 cm) in △CW, followed by RF, XGBoost, Cubist model, whereas the MARS and SVR ranked the lowest, such as SVR(R^2:0.41;RMSE:0.24 cm) in △DBH, SVR (R^2:0.43; RMSE:0.17 m) in △H, MARS (R^2:0.34;RMSE:0.20 cm) in △CW. In the validation set, the order of the accuracy of these models from high to low is CNN, RF, XGBoost, Cubist, MARS, and SVR in △DBH, CNN, RF, XGBoost, MARS, SVR, and Cubist in △H, CNN, XGBoost, RF, Cubist, SVR, and MARS in △CW.

Fig. 8 shows the residual plots of the training set and validation set of the △(DBH, H, CW) models established by SVR, MARS, Cubist, RF, XGBoost, and CNN regression models. In each plot, nearly all absolute values of the standard residuals based on training datasets and validation datasets are more condensed between –4 and 4, and the residuals of △DBH and △H models showed no significant trends, whereas residual plot from M2:MARS in △CW model did, which shows a clear trumpet shape. Compared to CNN, RF, XGBoost and Cubist, the SVR and MARS models' residuals are more dispersed. For combined model evaluation and residual plot, the CNN models in △(DBH, H, CW) had superior statistical performance in predicting △(DBH, H, CW) of Chinese fir, and could be selected for the 3-D Chinese fir dynamic growth visualization in our study.

D. 3-D Forest Dynamic Growth Visualization Based on CNN and SSP

We discovered that the reference tree's Ci and Ui had a significant influence on the annual increment of DBH, H, and CW based on CNN model. Wi and Mi were left out in the analysis due to no impact on △(DBH, H, CW). In our study, we have selected two very different growth scenes at the tree level based

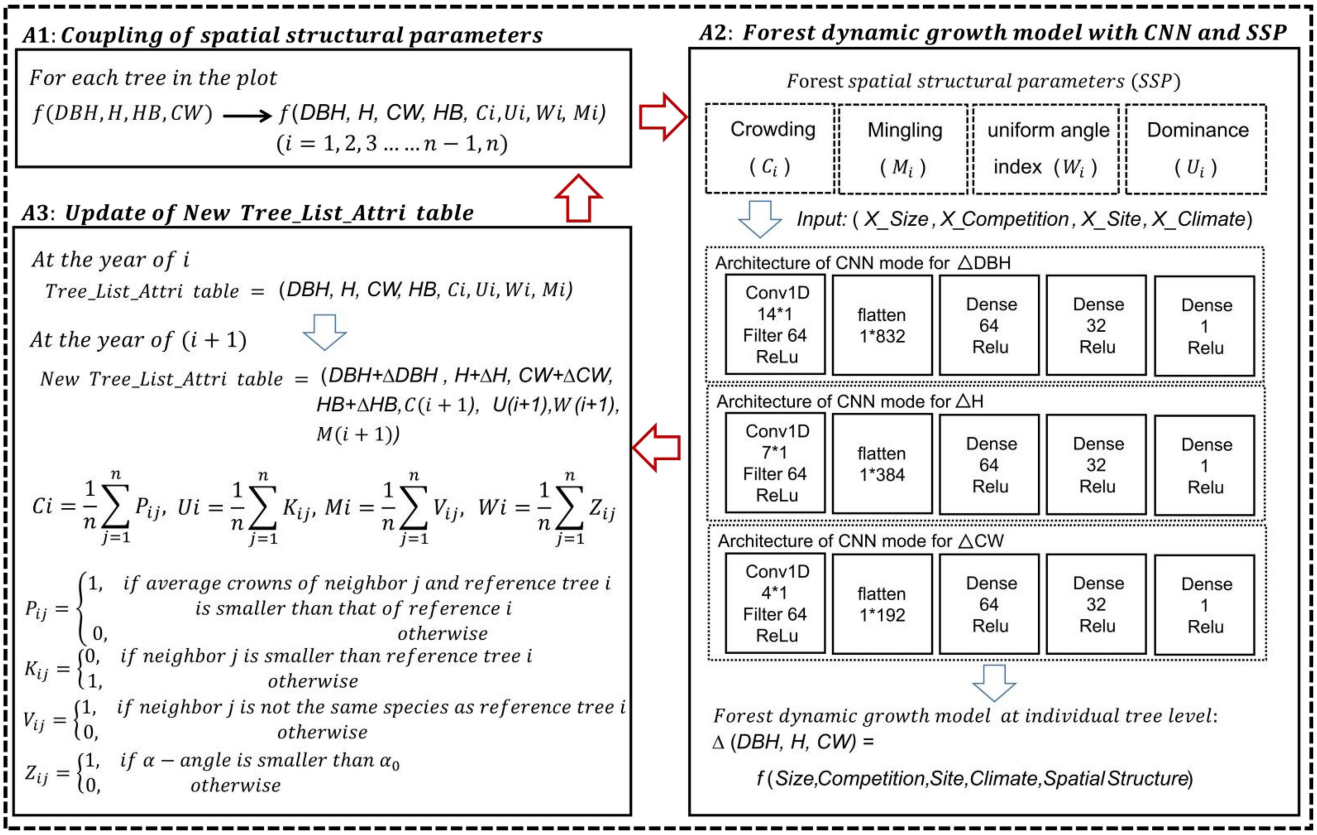

Fig. 5. Three Modules of FDGVM-CNN-SSP. Tree_List_Attri table was a DataTable in UE4 engine, which consists of the morphological data and spatial data for tree modeling, such as DBH, H, CW, HB, C, and U. X_Size, X_Competition, X_Site, X_Climate represent the independent variable from tree size, competition indices, site conditions, and climate factors. Wi is defined as the proportion of angles α smaller than the standard angle α_0 (72) and reflects the degree of uniformity of tree distribution. Mi is defined as the proportion of the four nearest neighbors that are of a different species than reference tree i. Ui is defined as the degree of DBH differentiation in this article and represents the relationship between the size of the reference tree i and its four nearest neighbors. Ci reflects the relationship between the canopy of the reference tree i and its four nearest neighbors and can reveal the degree of crowding of the reference tree i.

TABLE III
△(DBH, H, CW) PREDICTION ACCURACY OF TRAINING AND VALIDATION DATASETS

Models	△DBH						△H						△CW					
	Training Datasets			Validation Datasets			Training Datasets			Validation Datasets			Training Datasets			Validation Datasets		
	RMSE (cm)	MAE (cm)	R^2	RMSE (cm)	MAE (cm)	R^2	RMSE (m)	MAE (m)	R^2	RMSE (m)	MAE (m)	R^2	RMSE (m)	MAE (m)	R^2	RMSE (m)	MAE (m)	R^2
SVR	0.24	0.18	0.41	0.24	0.18	0.41	0.17	0.12	0.43	0.17	0.12	0.43	0.20	0.13	0.40	0.21	0.13	0.38
MARS	0.24	0.19	0.42	0.24	0.19	0.41	0.17	0.13	0.44	0.17	0.13	0.44	0.20	0.15	0.34	0.21	0.16	0.31
Cubist	0.21	0.14	0.56	0.21	0.13	0.55	0.17	0.11	0.45	0.17	0.11	0.42	0.19	0.13	0.41	0.20	0.13	0.39
RF	0.21	0.14	0.57	0.21	0.13	0.57	0.17	0.12	0.46	0.17	0.11	0.47	0.19	0.14	0.43	0.19	0.14	0.42
XGBoost	0.21	0.15	0.55	0.21	0.13	0.57	0.17	0.12	0.47	0.17	0.12	0.44	0.19	0.14	0.44	0.19	0.14	0.43
CNN	0.19	0.13	0.64	0.20	0.13	0.60	0.16	0.11	0.52	0.16	0.11	0.50	0.18	0.13	0.48	0.18	0.13	0.45

RF: random forest with all variables input; *N*: number of features used; RMSE: root-mean-square error; R^2: coefficient of determination.

on FDGVM-CNN-SSP as examples to demonstrate the growth changes at the year of 2018, 2020, and 2022 (see Fig. 9).

Based on FDGVM-CNN-SSP at stand level, we have selected plot 6 in Fig. 1 as our target stand to make a visual simulation of Chinese fir stands in the year 2018, 2020, and 2022 (see Fig. 10). According to the prediction model in A2 (see Fig. 5), we have calculated the values of △DBH, △H, and △CW at the year of 2018, 2020, and 2022 (see Table IV). According to A3 in Fig. 5, the values of DBH, H, CW of each tree in the scenes at the year of 2018, 2020, and 2022 were updated by adding the values of △DBH, △H, △CW at the year of 2018, 2020, 2022 into the values of DBH, H, and CW at the year of 2017, 2019, and 2021. C and U were recalculated with the change of CW and DBH at the end of this year (see Table IV). The red box in Fig. 10 clearly shows that the canopy is gradually turning from sparse to close at the year of 2018, 2020, and 2022.

IV. DISCUSSION

A. Feature Selection for FGMs

Dimensional difficulties arise with a large number of explanatory variables [38], necessitating the reduction of dimensions in

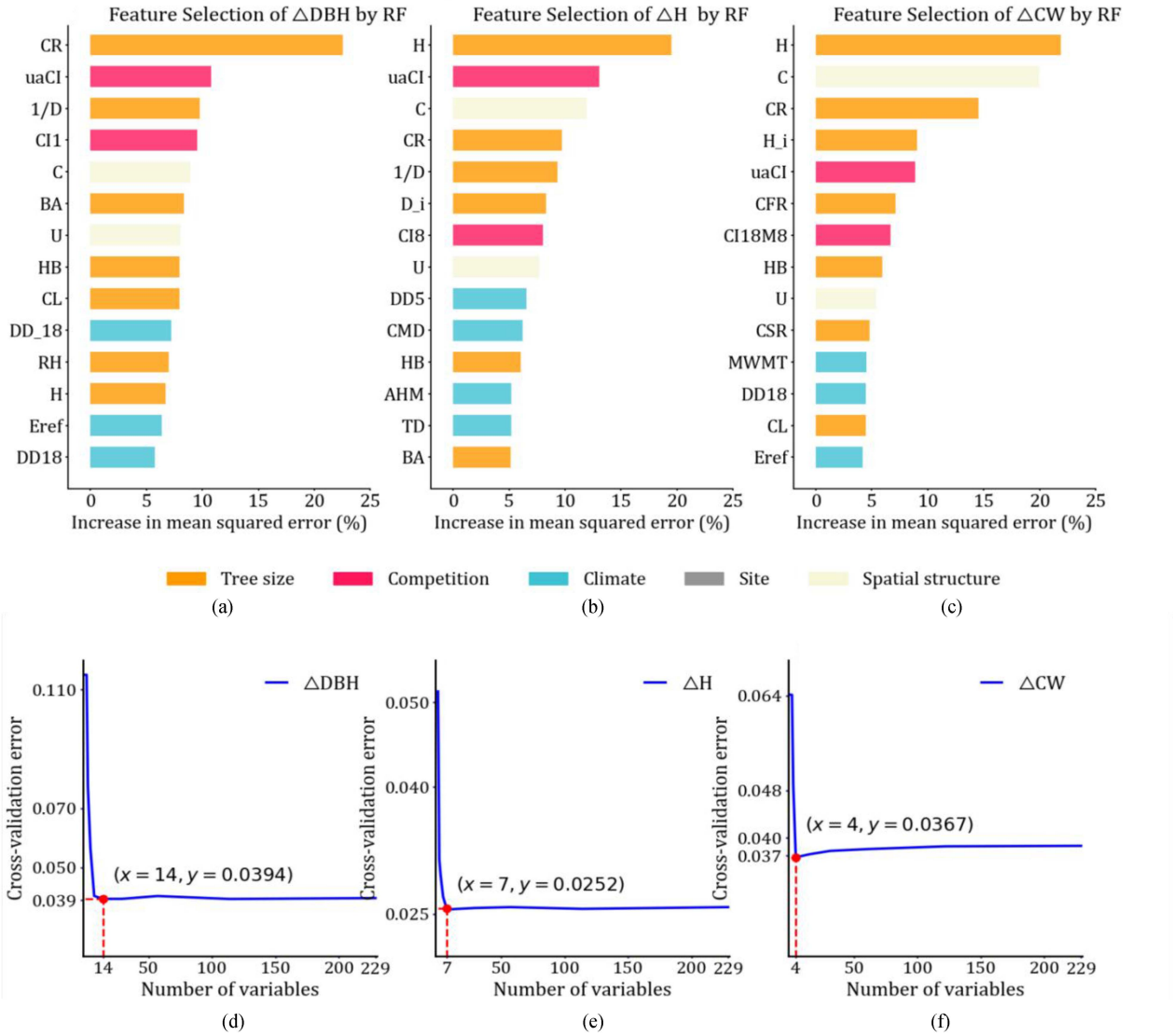

Fig. 6. Importance of difference features measured by % IncMSE (the percentage increase in the mean squared error) determination from 1000 runs of the RF for △(DBH, H, CW) in (a), (b), and (c). The graphs of (d), (e), and (f) represent the number of variables used and the average cross-validation error based on 10 times of 10-fold cross-validation. error.cv and n.var represent the cross-validation error and number of variables, respectively.

TABLE IV
COMPARISON OF PLOT CHARACTERISTIC BASED ON PREDICTED AND MEASURED

Type	year	DBH (cm)	△DBH(cm)	H (m)	△H (m)	CW (m)	△CW (m)	C	U
Measured	2017	22.55±4.09	——	16.49±1.65	——	4.43±0.76	——	0.89±0.18	0.47±0.35
Predicted	2018	23.17±4.29	0.62±0.24	17.34±1.72	0.85±0.10	4.87±0.79	0.45±0.23	0.90±0.14	0.48±0.36
Predicted	2019	23.76±4.52	0.59±0.28	18.21±1.81	0.88±0.12	5.23±0.85	0.35±0.22	0.91±0.12	0.48±0.36
Predicted	2020	24.37±4.78	0.61±0.30	19.12±1.95	0.91±0.16	5.59±0.94	0.36±0.22	0.92±0.08	0.48±0.36
Predicted	2021	24.98±5.04	0.61±0.31	20.04±2.10	0.91±0.18	5.94±1.04	0.35±0.21	0.92±0.07	0.48±0.36
Predicted	2022	25.61±5.32	0.63±0.32	21.00±2.31	0.97±0.24	6.30±1.19	0.36±0.24	0.93±0.06	0.48±0.36
Measured	2022	25.18±5.69	0.64±0.34	20.25±2.45	1.04±0.32	5.94±1.24	0.31±0.32	0.86± 0.14	0.48±0.36

Note: DBH, H, CW, C, and U are mean ± SD; DBH(%), H(%), and CW(%) represent the growth rate per year of DBH, H, and CW.

order to produce FGMs with reasonable accuracy [38], [39], [40]. In our study, the application of feature selection by RF and cross-validation reduced the number of variables and kept error metric lower from the initial solution to convergence, which decreased from 0.110 to 0.039 in △DBH, 0.050 to 0.025 in △H, and 0.064 to 0.037 in △CW. Our result corroborates earlier work such as of Luo et al. [56] and Sun et al. [57]. According to Fig. 5, we can found that CR, H, H have the largest contribution separately in △(DBH, H, CW), which is consistent with the result of Sharma and Breidenbach [15] and Sharma et al. [16].

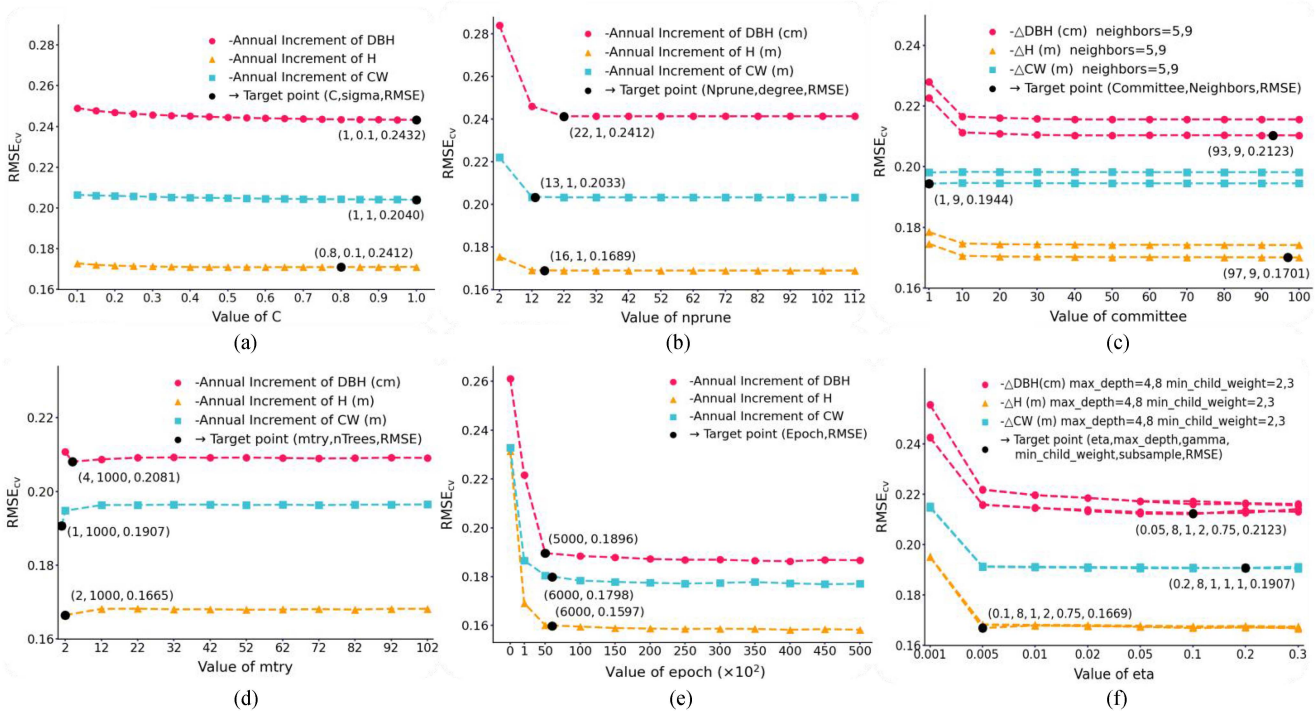

Fig. 7. Result of tuning parameters used for SVR, MARS, Cubist, RF, XGBoost, and CNN models training. The 10-fold cross-validation was used for validating. The black point is the target point, which represents the final value of parameters for each model. TuneGrid means user has to specify a tune grid manually. nprune is the maximum number of terms in the prune model. nTrees means the number of trees used in aggregation. nmtry means the number of variables to randomly sample as candidates at each split. Eta means the learning rate. (a) SVR. (b) MARS. (c) Cubist. (d) RF. (e) CNN. (f) XGBoost.

Through statistical analysis, the result shows that the variables CR, uaCI, and 1/D together account for 45.27% of the variance in △DBH. Similarly, the variables H, uaCI, and C account for 37.72% of variance in △H, and the variables CR, C, and CR account for 35.24% of variance in △CW. In addition, the result shows that the climate factors have a certain contribution on the forest growth, and the site factors have no significant effect on the growth model for site condition has not changed significantly during 2012–2017.

Apart from existing factors (e.g., tree size, competition indices, climate factors, site conditions) in FGMs, our study was the first to incorporate the spatial structural parameters independently into FGMs instead of integrating these spatial structural parameters into a comprehensive CI, which will cause the phenomenon of the same value of competition indices with different spatial structure conditions. Therefore, the analysis of spatial structural parameters' effect on forest stand is a supplement to the relationship between CI and forest growth. As we can see, the result of the importance ranking from Fig. 6, the spatial structural parameters C and U have a great contribution in △(DBH, H, CW). Through the statistical analysis, the spatial structural parameters C and U have a certain contribution to the forest growth, and the C and U can explain 21.5%, 15.23%, and 9.32% of the variance in △(DBH, H, CW) models, respectively.

Competition indices play an important role in FGM [58]. However, it becomes rather challenging to determine the optimal CI for the growth model because the success of competition indices will change as a result of stand conditions. Therefore, we have selected nine distance-independent competition metrics (CI1–CI9), 11 distance-dependent ones (CI10–CI20), and eight methods of determining competitors (M1–M8) to determine the best competition indices with specified methods in FGM. The result shows that uaCI (CI20) has the largest contribution among competition indices and that the growth model with spatial competition indices has a better performance than with nonspatial ones (see Fig. 6), which is consistent with Maleki et al. [23] and Sharma and Breidenbach [15]. In the process of feature selection for △(DBH, H, CW) model, we have found that there is no one method is superior to other methods, and the relative importance percentage values are distributed around 0.5%, which support the work of Kuehne et al. [59] and Zhou et al. [60] (see Fig. 13).

B. *Hyperparameter Tuning and Model Selection*

Hyperparameter tuning for machine learning models is a fundamental procedure that affects FGMs prediction performance [61]. Therefore, in order to get a reliable performance of FGMs for a virtual forest, their hyperparameters must be optimized. Grid search, as one of the most common approaches for hyperparameters optimization, has been employed in our study [61]. In order to balance model predictive performance and computing costs, the value of ntree in RF was set to 1000. Our study found that the performance of RF decreased with the

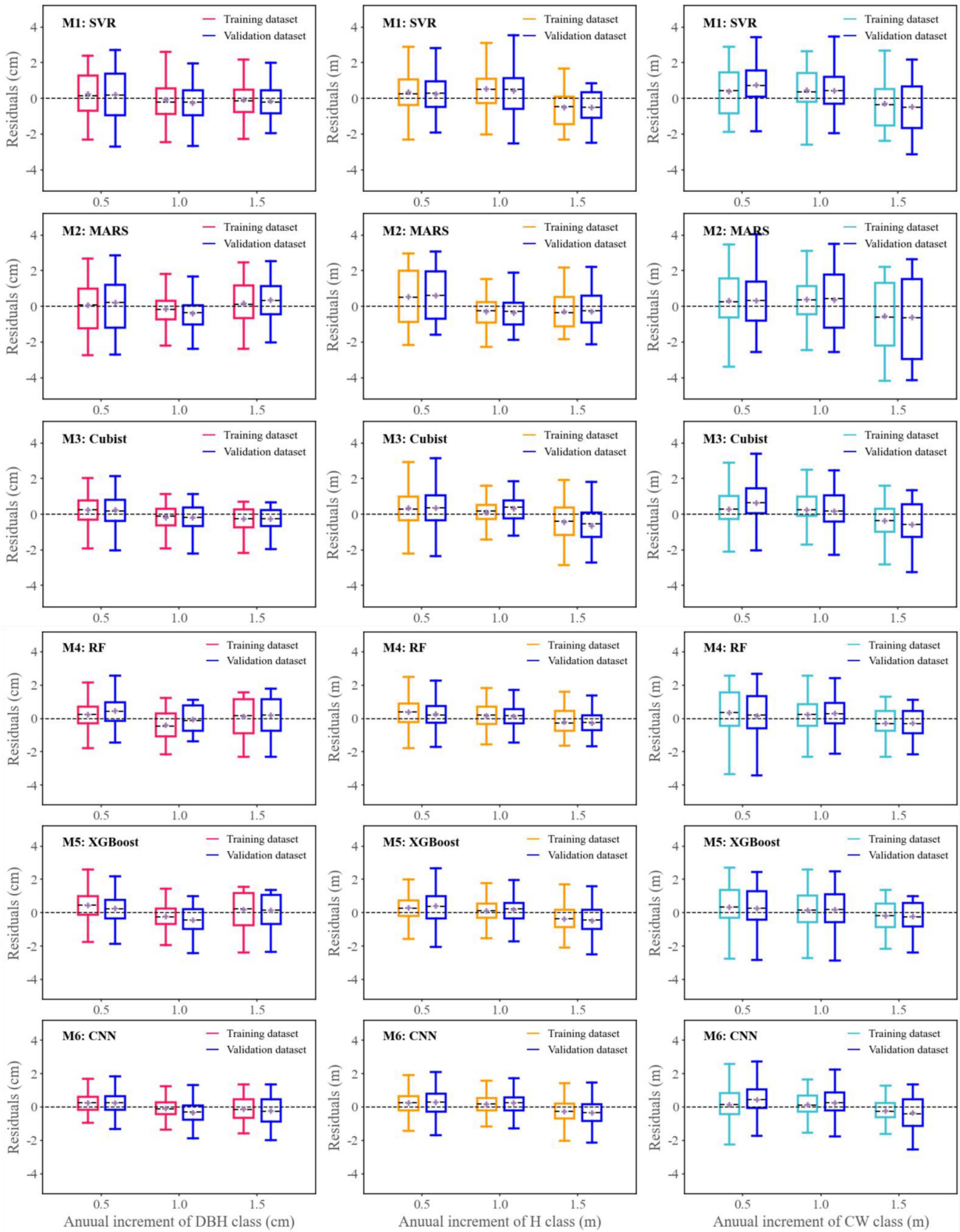

Fig. 8. Box plots of standard residuals of △(DBH, H, CW) models by SVR, MARS, Cubist, RF, XGBoost, and CNN. The box length, whisker length, horizontal lines in red, and plus signs in a box represent the interquartile range (IQR); the class minimum and maximum values in the IQR; and the class median and mean values, respectively. △(DBH, H, CW) represents annual increment of DBH, H, and CW, separately.

Fig. 9. Two trees growth based on FDGVM-CNN-SSP. (a)–(c) Growth process of the treeID No. 1 at the year of 2018, 2020, 2022; (d)–(f) Growth process of the treeID No. 198 at the year of 2018, 2020, 2022. i means the reference tree; a, b, c, d mean the four nearest tree of the reference tree i in the plot.

increasing of mtry ($4 < \text{mtry} < 102$), whereas the value of C in SVR, nprune in MARS, committee in Cubist, epoch in CNN, eta in XGBoost shows the opposite result when the sigma = 0.1 in SVR, degree = 1 in MARS, neighbors = 5/9 in Cubist, max_depth = 4/8, child_weight = 2/3, gamma = 1 in XGBoost models. The result shows that the hyperparamter has a significant effect on model accuracy and more attention should be paid to this critical step.

CNNs have been commonly used to process the tasks of object classification and detection, speech recognition, and natural language processing [55], while fewer in regression model. Differing from typical shallow learning algorithms, CNN extracts complicated characteristics from input data and transforms the features of the trees in the original space to a new feature. In addition, CNN can make full use of neighborhood information, discover multiple levels of representations from input data, reveal the deep features, and distinguish the differences between data in different units. So, we have introduced the CNN model to learn the relationship between the selected features in Fig. 6 with △(DBH, H, CW) for regression of FGMs in our study. According to the result of Table III, we have found that CNN regression model had a better performance of predicting annual increment of growth in forest, comparing other machine learning methods with the same input variables, which is consistent with the work of Qin et al. [40]. For example, compared to SVR, MARS, Cubist, RF, and XGBoost, CNN model has the highest value of R^2 and the lowest value of RMSE, MAE with 0.64, 0.19 cm, 0.13 cm in △DBH model; 0.52, 0.16 m, 0.11 m in △H

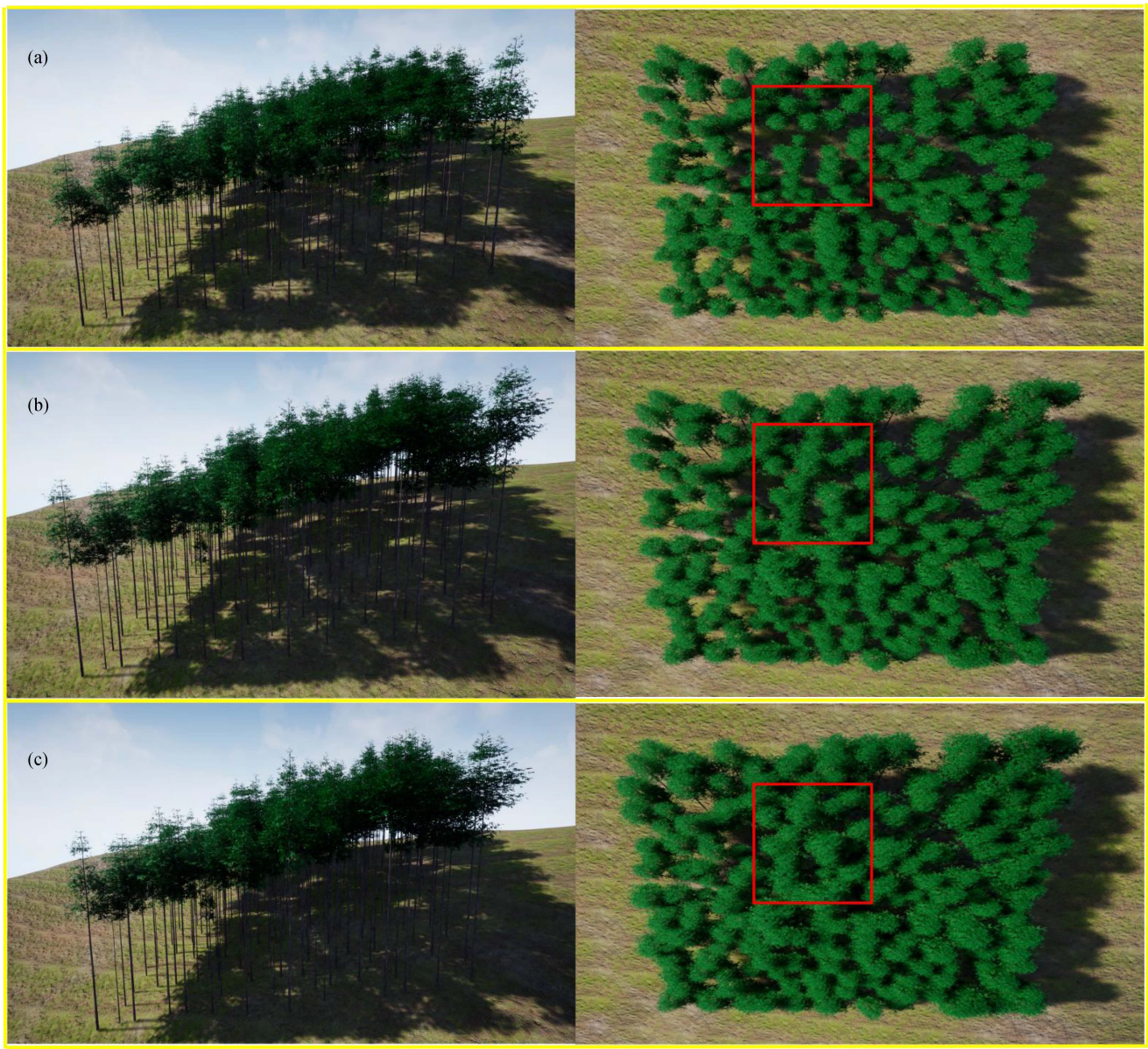

Fig. 10. Growth process of Chinese fir stands based on FDGVM-CNN-SSP. (a) Visual simulation of 22-year-old Chinese fir stands at 2018. (b) Visual simulation of 24-year-old Chinese fir stands at 2020. (c) Visual simulation of 26-year-old Chinese fir stands at 2022. The left panel shows the side view observation angle of the stand visual simulation, and the right panel shows the top view observation angle.

model; and 0.48, 0.18 m, 0.13 m in △CW model. The result also indicates that the CNN model has promising applications in forestry statistical regression analysis.

C. 3-D Forest Dynamic Growth Modeling

In a virtual forest, trees are crucial components of the natural environment and their growth and development is complex, particularly in a highly heterogeneous forest stand [62]. However, current forest growth visual methods are generally based on the plot or stand level without adding the constraints of the spatial structure parameters in a microenvironment [3], [4], which cannot meet the visual demand for individual tree growth and development information. Therefore, our research has proposed a method of FDGVM-CNN-SSP by incorporating the spatial structural parameter crowding (C) and dominance (U) based on deep learning technique. Unlike the visual method of growth at stand level, the method of FDGVM-CNN-SSP can comprehensively express the information of growth and development at individual tree level and stand level, avoiding the phenomenon of each tree in the forest stand with the same growth increment, and well meets the application and scientific research purposes of forest growth visualization platform. By adding the constraint conditions of spatial structure in FDGVM-CNN-SSP, the visual simulation of growth and development under highly heterogeneous forest conditions

can be more realistic, and the uncertainty problem caused by spatial environment differences can be reduced. However, our method FDGVM-CNN-SSP is restricted to the stable and undisturbed forest environment, and its capacity to reflect spatial structure changes induced by human disturbance and natural succession is limited, owing to the trees' slow response to disturbance.

In order to further discuss the feasibility of FDGVM-CNN-SSP, we have selected the determination of coefficient (R^2) and RMSE as the metrics to make an analysis of the individual trees' characteristics based on measured and predicted (see Fig. 14). According to Fig. 14, we can see the difference in DBH and H of predicted and measured is acceptable in our research, which shows that R^2, RMSE in DBH is 86.8%, 2.062 cm, and in H is 79.2%, 1.114 m separately. The trend of DBH and H distribution is similar, which is mainly distributed in 20–30 cm and 16–24 m, respectively. The difference in CW of predicted and measured exists, which results in the difference in inconformity of spatial structure in crowding (C). The result may be caused by different response mechanism of tree crown to natural disturbance, such as extreme drought and rainfall in Youxian County during 2018–2022. Through the statistical analysis, we have found that the difference between predicted and measured data is not significant, and the method of FDGVM-DL-SSP has a certain applicability in a heterogeneous forest environment.

V. Conclusion

This study provides a new approach for 3-D forest dynamic growth visualization method FDGVM-CNN-SSP. The highlights of the approach FDGVM-CNN-SSP are as follows. 1) Spatial structural parameters crowding (C) and dominance (U) were incorporated into the FGMs of DBH, H, and CW at individual tree level. 2) The CNN regression model was introduced into the FGMs of DBH, H, and CW at individual tree level for higher precision and relationship mining among multiple variables. According to statistical analysis of FDGVM-CNN-SSP, we found that the following conditions hold.

1) The spatial structural parameters C and U have a certain contribution to the individual tree growth, and C and U can explain 21.5%, 15.23%, and 9.32% of the variance in DBH, H, and CW growth models, respectively.
2) Our method based on CNN exhibits competitive prediction performance with R^2, RMSE 0.64 cm, 0.19 cm in △DBH model, 0.52 m, 0.16 m in △H model, and 0.48, 0.18 m in △CW model when compared with machine learning algorithm RF, SVR, KNN, MARS, and XGBoost.
3) Our method can achieve the visual simulation of Chinese fir plantations at individual tree level and stand level and well meets the visual demand for individual tree growth and development information.

Appendix

Variables Type	Symbol	Description	Method
Tree size	DBH	Diameter at breast height	Directed Measurement
	H	Total height	Directed Measurement
	CW	Average crown width	Directed Measurement
	HB	Crown base height	Directed Measurement
	CL	crown length	CL= H-HB
	CR	Crown Ratio	CR = CL/H
	CSR	Crown shape ratio	CSR= CW/H
	CFR	Crown fullness ratio	CFR=CW/CL
	△DBH	Annual increment of DBH	△DBH= DBH_{i+1}-DBH_i, i means the year
	△H	Annual increment of H	△H= H_{i+1}-H_i, i means the year
	△CW	Annual increment of CW	△CW= CW_{i+1}-CW_i, i means the year
	△HB	Annual increment of HB	△HB= HB_{i+1}-HB_i, i means the year
	logDBH	Logarithmic of DBH	logDBH=$\log_{10}$DBH
	logH	Logarithmic of H	logH=$\log_{10}$H
	logCW	Logarithmic of CW	logCW=$\log_{10}$CW
	logHB	Logarithmic of HB	logHB=$\log_{10}$HB
	DBH^2	Square of DBH	DBH^2=DBH*DBH
	H^2	Square of H	H^2=H*H
	CW^2	Square of CW	CW^2=CW*CW
	HB^2	Square of HB	HB^2=HB*HB
	$DBH^{1/2}$	Square root of DBH	$DBH^{1/2}$
	$H^{1/2}$	Square root of H	$H^{1/2}$
	$CW^{1/2}$	Square root of CW	$CW^{1/2}$
	$HB^{1/2}$	Square root of HB	$HB^{1/2}$
	1/DBH	Reciprocal of DBH	1/DBH
	1/H	Reciprocal of H	1/H
	1/CW	Reciprocal of CW	1/CW
	1/HB	Reciprocal of HB	1/HB

Fig. 11. Variables descriptions and calculation method of tree size.

Source	Competition index formula	Source	Competition index formula
Distance-independent competition indices:		Distance-dependent competition indices :	
Wykoff et al.(1982)	$CI_1 = BAL_i = \left(\sum_{d_i<d_j}^{n} g_i\right)\Big/ S$	Staebler(1951)	$CI_{10} = \sum_{j=1}^{n}(\frac{OL_{ij} \times CR_i}{2})$
Lorimer (1983)	$CI_2 = [(\sum_{j\neq 1}^{n} d_j)\Big/ d_i]/S$	Newnham (1966)	$CI_{11} = \frac{1}{2\pi}\sum_{j=1}^{n}\theta_{ij}$
Hamilton(1986)	$CI_3 = \frac{d_i}{d_j}$	Gerrard(1969)	$CI_{12} = \frac{1}{Z_i}\sum_{j=1}^{n}\theta_{ij}$
Tomé and Burkhart (1989)	$CI_4 = \frac{d_i}{d_{max}}$	Bella(1971)	$CI_{13} = \sum_{j=1}^{n}\left(\frac{O_{ij}}{Z_i}\right)\left(\frac{d_j}{d_i}\right)^{EX}$
Tomé and Burkhart (1989)	$CI_5 = \frac{g_i}{\bar{g}}$	Arney(1973)	$CI_{14} = \left\{\left[\sum_{j=1}^{n}(O_{ij} + Z_j)\right]\Big/ Z_i\right\} \times 100$
Tomé and Burkhart (1989)	$CI_6 = \frac{g_i}{g_{max}}$	Hegyi (1974)	$CI_{15} = \sum_{j=1}^{n}(\frac{d_j}{d_i} \times \frac{1}{L_{ij}})$
Corona and Ferrara (1989)	$CI_7 = [(\sum_{j\neq 1}^{n} g_j)\Big/ g_i]/S$	Sun (1977)	$CI_{16} = \sum_{j=1}^{n}(\frac{ca_i}{ca_j} \times \frac{d_j}{d_i} \times \frac{1}{L_{ij}})$
Schröder and Gadow (1999)	$CI_8 = [(\sum_{d_i<d_j}^{n} g_j)\Big/ G\,]/RS$	Alemdağ (1978)	$CI_{17} = \sum_{j=1}^{n}\left\{\pi(\frac{L_{ij} \times d_i}{d_i + d_j})^2\left[\frac{d_j/L_{ij}}{\sum(d_j/L_{ij})}\right]\right\}$
Nagel(1999)	$CI_9 = (\sum_{1}^{n} hca_{j(HWCW_i)})/S$	Martin and EK(1984)	$CI_{18} = \sum_{j=1}^{n}\left(\frac{d_j}{d_i}\right) \times e^{(16\times L_{ij})/(d_i+d_j)}$
		Ritchie and Hamann (1985)	$CI_{19} = \frac{1}{4 \times 43560}\sum CD_j^2(hcb_j) \cdot \pi \cdot 100$
		Hui G Y (2013)	$CI_{20} = \frac{1}{n}\sum_{j=1}^{n}\frac{(\alpha_1 + \alpha_2 \cdot c_{ij})_j}{180^\circ} \cdot U_i$

Fig. 12. Distant-independent and distance-dependent competition indices used in our study for growth modeling. CI1–CI20 represent 20 competition indices; i, j represent the subject tree and competitor tree respectively; BAL_i is basal area of trees larger than the subject tree (m^2/ha); d_i, d_j, d_{max} mean DBH of subject tree and competitor tree (cm), and maximum DBH in the sample plot; S is plot area (ha); g_i, $\bar{g}$, g_{max}, g_j, G represent basal area of subject tree (m^2/ha), mean basal area of sample plot (m^2/ha), basal area of the thickest diameter in the sample plot (m^2/ha), basal area of competition tree (m^2/ha), and basal area of the trees within the plot (m^2/ha) separately; RS is relative spacing index of plot; hca_j, $HWCW_i$ mean tree horizontal crown area (m^2) and height of greatest crown width in 66% of subject tree height (m); OL_{ij}, CR_i mean distance of crown projection overlap between subject tree i and competitor tree j (m^2) and crown radius of subject tree i (m); θ_{ij} is the interior angle subtended for treei's circle by competitor j's overlap zone (in radians); Z_i, Z_j mean the area of influence zone of subject tree and competitor tree (m^2); O_{ij} is crown overlap between the neighbor tree j and the subject tree i (m^2); L_{ij} is distance of crown projection overlap between subject tree i and competitor tree j (m^2); ca_i, ca_j mean crown area of subject tree i (m^2) and competitor tree j (m^2); EX is exponential factor (EX = 1 in our study); hcb_j is crown base height of competitor tree j (m); $CD_j(hcb_j)$ is crown diameter at crown base height of competitor tree j; α_1 is arctg(H_i/d_{ij}), if the neighbor tree j is higher than reference tree i, else is arctg(H_j/d_{ij}); α_2 is arctg((H_j-H_i)/d_{ij}); c_{ij} is the value of 1, if the neighbor tree j is higher than reference tree i, else is the value of 0; U_i is the dominance of reference tree i.

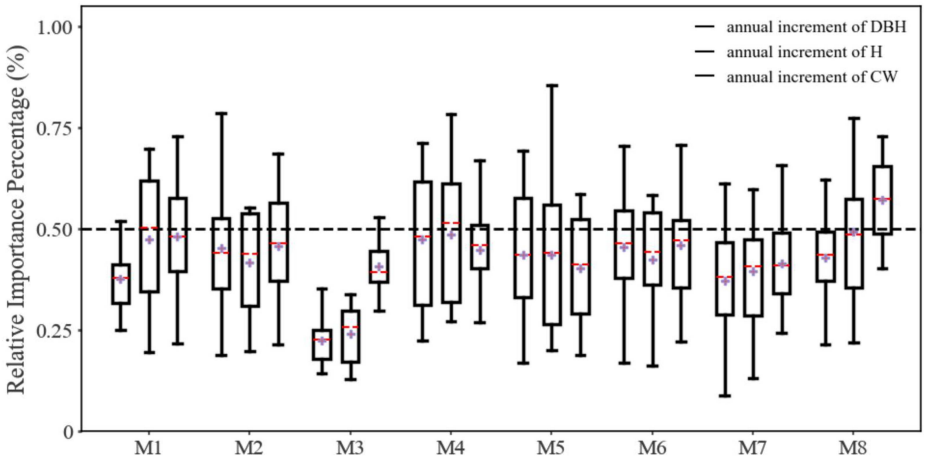

Fig. 13. Box plots of relative importance percentage of eight methods determining the influence zone. The box length, whisker length, horizontal lines in red, and plus signs in a box represent the IQR; the class minimum and maximum values in the IQR, and the class median and mean values, respectively.

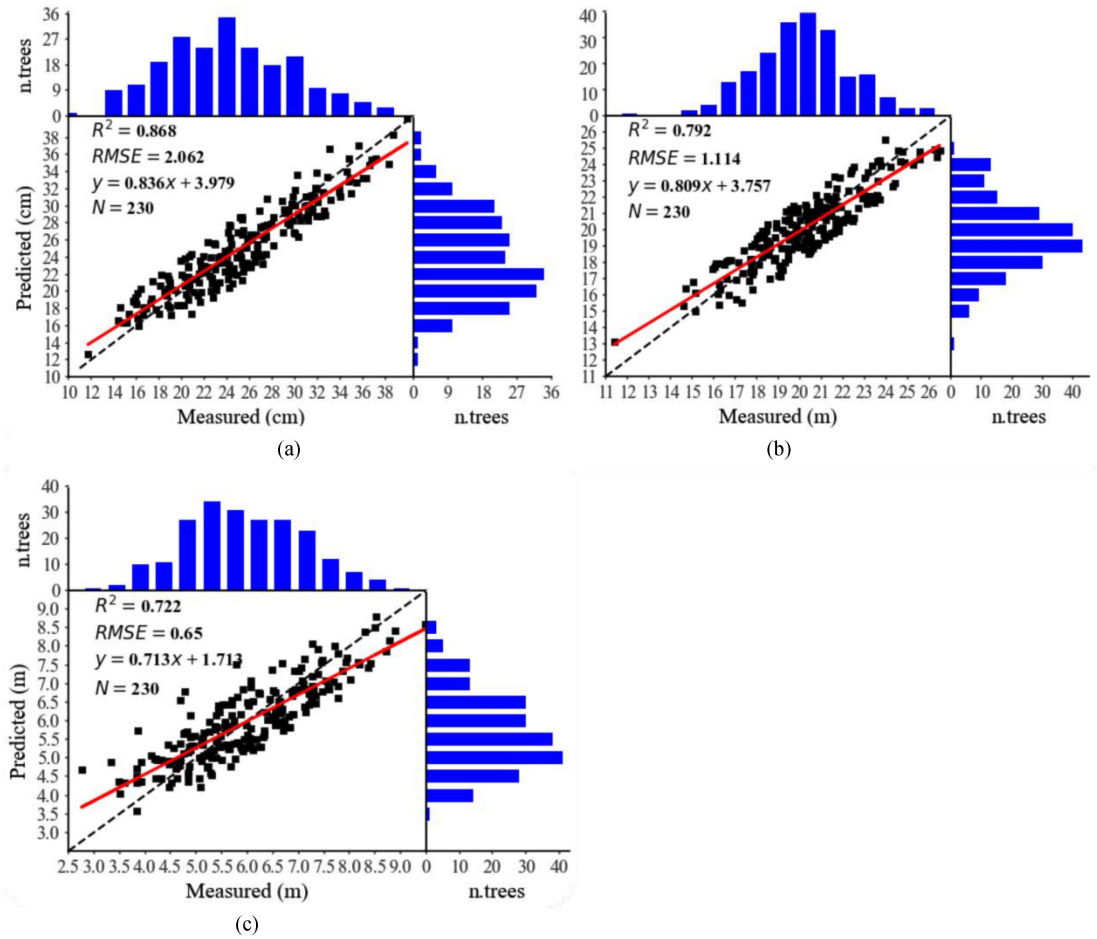

Fig. 14. Comparison between measured and predicted values of DBH, H, and CW for 26-years-old Chinese fir stand at the year 2022. The red solid lines indicate the regression fitting result. The bar plot in the top and right of the picture is the number distribution of measured and predicted at class of DBH, H, and CW. n.trees represents the number of trees at different class. *N* is the number of plot trees. (a) DBH. (b) H. (C) CW.

ACKNOWLEDGMENT

The authors would like to thank the teammates who helped collected field data and its processing.

REFERENCES

[1] J. Uusitalo and B. Orland, "Virtual forest management: Possibilities and challenges," *Int. J. Forest Eng.*, vol. 12, no. 2, pp. 57–66, 2001.

[2] L. Tang, X. Peng, C. Chen, H. Huang, and D. Lin, "Three-dimensional forest growth simulation in virtual geographic environments," *Earth Sci. Rev.*, vol. 12, pp. 31–41, 2019.

[3] X. Hu et al., "Visual simulation research on growth polymorphism of Chinese fir stand based on different comprehensive grade models of spatial structure parameters," *Forests*, vol. 14, no. 3, 2023, Art. no. 617.

[4] K. Lei et al., "A novel strategy for constructing large-scale forest scene: Integrating forest hierarchical models and tree growth models to improve the efficiency and stability of forest polymorphism simulation," *Forests*, vol. 14, no. 8, 2023, Art. no. 1595.

[5] M. Fabrika, P. Valent, and Ľ. Scheer, "Thinning trainer based on forest-growth model, virtual reality and computer-aided virtual environment," *Environ. Model. Softw.*, vol. 100, pp. 11–23, 2018.

[6] A. Porte and H. Bartelink, "Modelling mixed forest growth: A review of models for forest management," *Ecol. Model.*, vol. 150, no. 1/2, pp. 141–188, 2002.

[7] H. Pretzsch, *Forest Dynamics, Growth, and Yield*. Berlin, Germany: Springer, 2009.

[8] Z. Ma, H. Zhang, Y. Li, T. Yang, R. Huang, and S. Li, "3D visual simulation of Chinese fir based on the influence of different stand spatial structures," in *Proc. IEEE 2nd Int. Conf. Image, Vis. Comput.*, 2017, pp. 559–565.

[9] S. Li, H. Zhang, Y. Li, T. Yang, and K. Shen, "Three-dimensional visualization simulation of Chinese Fir stand growth based on unity3D," in *Proc. IEEE 3rd Int. Conf. Mech., Control Comput. Eng.*, 2018, pp. 530–534.

[10] N. Fahlvik and K. Nyström, "Models for predicting individual tree height increment and tree diameter in young stands in southern Sweden," *Scand. J. Forest Res.*, vol. 21, no. S7, pp. 16–28, 2006.

[11] F. C. Uzoh and W. W. Oliver, "Individual tree height increment model for managed even-aged stands of ponderosa pine throughout the western United States using linear mixed effects models," *Forest Ecol. Manage.*, vol. 221, no. 1–3, pp. 147–154, 2006.

[12] P. Adame, J. Hynynen, I. Canellas, and M. del Río, "Individual-tree diameter growth model for rebollo oak (Quercus pyrenaica Willd.) coppices," *Forest Ecol. Manage.*, vol. 255, no. 3/4, pp. 1011–1022, 2008.

[13] W. Ma and X. Lei, "Nonlinear simultaneous equations for individual-tree diameter growth and mortality model of natural Mongolian oak forests in northeast China," *Forests*, vol. 6, no. 6, pp. 2261–2280, 2015.

[14] F. C. Uzoh and W. W. Oliver, "Individual tree diameter increment model for managed even-aged stands of ponderosa pine throughout the western United States using a multilevel linear mixed effects model," *Forest Ecol. Manage.*, vol. 256, no. 3, pp. 438–445, 2008.

[15] R. P. Sharma and J. Breidenbach, "Modeling height-diameter relationships for Norway spruce, Scots pine, and downy birch using Norwegian national forest inventory data," *Forest Sci. Technol.*, vol. 11, no. 1, pp. 44–53, 2015.

[16] R. P. Sharma, Z. Vacek, and S. Vacek, "Modeling individual tree height to diameter ratio for Norway spruce and European beech in Czech Republic," *Trees*, vol. 30, pp. 1969–1982, 2016.

[17] R. Buchacher and T. Ledermann, "Interregional crown width models for individual trees growing in pure and mixed stands in Austria," *Forests*, vol. 11, no. 1, 2020, Art. no. 114.
[18] R. Bałazy, A. Kamińska, M. Ciesielski, J. Socha, and M. Pierzchalski, "Modeling the effect of environmental and topographic variables affecting the height increment of Norway spruce stands in mountainous conditions with the use of LiDAR data," *Remote Sens.*, vol. 11, no. 20, 2019, Art. no. 2407.
[19] S. Etzold et al., "Nitrogen deposition is the most important environmental driver of growth of pure, even-aged and managed European forests," *Forest Ecol. Manage.*, vol. 458, 2020, Art. no. 117762.
[20] H. Wu et al., "Tree growth rate and soil nutrient status determine the shift in nutrient-use strategy of Chinese fir plantations along a chronosequence," *Forest Ecol. Manage.*, vol. 460, 2020, Art. no. 117896.
[21] O. Junttila, "Effects of temperature on shoot growth in northern provenances of Pinus sylvestris L," *Tree Physiol.*, vol. 1, no. 2, pp. 185–192, 1986.
[22] Y. Messaoud and H. Chen, "The influence of recent climate change on tree height growth differs with species and spatial environment," *PLoS One*, vol. 6, no. 2, 2011, Art. no. e14691.
[23] K. Maleki, A. Kiviste, and H. Korjus, "Analysis of individual tree competition on diameter growth of silver birch in Estonia," *Forest Syst.*, vol. 24, no. 2, 2015, Art. no. e023.
[24] R. P. Sharma, Z. Vacek, and S. Vacek, "Individual tree crown width models for Norway spruce and European beech in Czech Republic," *Forest Ecol. Manage.*, vol. 366, pp. 208–220, 2016.
[25] L. Zhang, G. Hui, Y. Hu, and Z. Zhao, "Spatial structural characteristics of forests dominated by Pinus tabulaeformis Carr," *PLoS One*, vol. 13, no. 4, 2018, Art. no. e0194710.
[26] T. Zhang, X. Dong, H. Guan, Y. Meng, J. Ruan, and Z. Wang, "Effect of thinning on the spatial structure of a Larix gmelinii Rupr. secondary forest in the Greater Khingan Mountains," *Forests*, vol. 9, no. 11, 2018, Art. no. 720.
[27] X. Zhang, Y. Wang, Y. Wang, S. Zhang, and X. Zhao, "Effects of social position and competition on tree transpiration of a natural mixed forest in Chongqing, China," *Trees*, vol. 33, pp. 719–732, 2019.
[28] K. Lei et al., "Comprehensive decision index of logging (CDIL) and visual simulation based on horizontal and vertical structure parameters," *Forests*, vol. 14, no. 2, 2023, Art. no. 277.
[29] F. Cortini, C. N. Filipescu, A. Groot, D. A. MacIsaac, and T. Nunifu, "Regional models of diameter as a function of individual tree attributes, climate and site characteristics for six major tree species in Alberta, Canada," *Forests*, vol. 2, no. 4, pp. 814–831, 2011.
[30] M. Toledo et al., "Climate is a stronger driver of tree and forest growth rates than soil and disturbance," *J. Ecol.*, vol. 99, no. 1, pp. 254–264, 2011.
[31] N. Subedi and M. Sharma, "Climate-diameter growth relationships of black spruce and jack pine trees in boreal Ontario, Canada," *Glob. Change Biol.*, vol. 19, no. 2, pp. 505–516, 2013.
[32] L. Chen et al., "Drought explains variation in the radial growth of white spruce in western Canada," *Agricultural Forest Meteorol.*, vol. 233, pp. 133–142, 2017.
[33] L. Wang, H. Zhang, H. Zhang, T. Yang, J. Zhang, and Y. Liu, "A novel 3D tree-modeling method of incorporating small-scale spatial structure parameters in a heterogeneous forest environment," *Forests*, vol. 14, no. 3, 2023, Art. no. 639.
[34] M. I. Ashraf, Z. Zhao, C. P. A. Bourque, D. A. MacLean, and F. Meng, "Integrating biophysical controls in forest growth and yield predictions with artificial intelligence technology," *Can. J. Forest Res.*, vol. 43, no. 12, pp. 1162–1171, 2013.
[35] S. K. Hamidi, E. K. Zenner, M. Bayat, and A. Fallah, "Analysis of plot-level volume increment models developed from machine learning methods applied to an uneven-aged mixed forest," *Ann. Forest Sci.*, vol. 78, pp. 1–16, 2021.
[36] Q. Ou, X. Lei, and C. Shen, "Individual tree diameter growth models of larch–spruce–fir mixed forests based on machine learning algorithms," *Forests*, vol. 10, no. 2, 2019, Art. no. 187.
[37] R. Cheng, J. Zhang, X. Wang, Z. Ge, and Z. Zhang, "Predicting the growth suitability of Larix principis-rupprechtii Mayr based on site index under different climatic scenarios," *Front. Plant Sci.*, vol. 14, 2023, Art. no. 1097688.
[38] S. B. Kukuk and Z. H. Kilimci, "Comprehensive analysis of forest fire detection using deep learning models and conventional machine learning algorithms," *Int. J. Comput. Exp. Sci. Eng.*, vol. 7, no. 2, pp. 84–94, 2021.
[39] G. F. Bueno, E. A. Costa, C. A. G. Finger, V. Liesenberg, and P. C. Bispo, "Machine learning: Crown diameter predictive modeling for open-grown trees in the Cerrado biome, Brazil," *Forests*, vol. 13, no. 8, 2022, Art. no. 1295.
[40] Y. Qin, B. Wu, X. Lei, and L. Feng, "Prediction of tree crown width in natural mixed forests using deep learning algorithm," *Forest Ecosyst.*, vol. 10, 2023, Art. no. 100109.
[41] G. R. Staebler, *Growth and Spacing in an Even-Aged Stand of Douglas-Fir*. Ann Arbor, MI, USA: Univ. Michigan Press, 1951, doi: 10.5735/085.046.0409.
[42] A. Sims, A. Kiviste, M. Hordo, D. Laarmann, and K. von Gadow, "Estimating tree survival: A study based on the Estonian forest research plots network," *Annales Botanici Fennici*, vol. 46, no. 4, pp. 336–352, 2009.
[43] W. Btterlich, "Die Winkelzählprobe: Ein optisches Meßverfahren zur raschen Aufnahme besonders gearteter Probeflächen für die Bestimmung der Kreisflächen pro Hektar an stehenden Waldbeständen," *Forstwissenschaftliches Centralblatt*, vol. 71, no. 7/8, pp. 215–225, 1952.
[44] M. Richards, A. J. S. McDonald, and M. Aitkenhead, "Optimisation of competition indices using simulated annealing and artificial neural networks," *Ecol. Model.*, vol. 214, no. 2–4, pp. 375–384, 2008.
[45] K. Von Gadow and G. Y. Hui, *Characterizing Forest Spatial Structure and Diversity*. Lund, Sweden: Univ. Lund Press, 2002, pp. 20–30.
[46] A. Okabe, B. Boots, K. Sugihara, and S. N. Chiu, *Spatial Tessellations: Concepts and Appl. of Voronoi Diagrams*. Hoboken, NJ, USA: Wiley, 2009.
[47] L. P. Leites, A. P. Robinson, G. E. Rehfeldt, J. D. Marshall, and N. L. Crookston, "Height-growth response to climatic changes differs among populations of Douglas-fir: A novel analysis of historic data," *Ecol. Appl.*, vol. 22, no. 1, pp. 154–165, 2012.
[48] M. Żywiec, E. Muter, T. Zielonka, M. Delibes, G. Calvo, and J. M. Fedriani, "Long-term effect of temperature and precipitation on radial growth in a threatened thermo-Mediterranean tree population," *Trees*, vol. 31, pp. 491–501, 2017.
[49] S. E. Russo, S. J. Davies, D. A. King, and S. Tan, "Soil-related performance variation and distributions of tree species in a Bornean rain forest," *J. Ecol.*, vol. 93, no. 5, pp. 879–889, 2005.
[50] H. Pretzsch and E. K. Zenner, "Toward managing mixed-species stands: From parametrization to prescription," *Forest Ecosyst.*, vol. 4, pp. 1–17, 2017.
[51] G. Hui, G. Zhang, Z. Zhao, and A. Yang, "Methods of forest structure research: A review," *Curr. Forestry Rep.*, vol. 5, pp. 142–154, 2019.
[52] C. Strobl, A. L. Boulesteix, T. Kneib, T. Augustin, and A. Zeileis, "Conditional variable importance for random forests," *BMC Bioinf.*, vol. 9, pp. 1–11, 2008.
[53] R Core Team, "R: A language and environment for statistical computing," 2013. [Online]. Available: https://www.r-project.org/
[54] T. M. Carvajal, K. M. Viacrusis, L. F. T. Hernandez, H. T. Ho, D. M. Amalin, and K. Watanabe, "Machine learning methods reveal the temporal pattern of dengue incidence using meteorological factors in metropolitan Manila, Philippines," *BMC Infect. Dis.*, vol. 18, no. 1, pp. 1–15, 2018.
[55] Y. LeCun, Y. Bengio, and G. Hinton, "Deep learning," *Nature*, vol. 521, no. 7553, pp. 436–444, 2015.
[56] M. Luo et al., "Combination of feature selection and CatBoost for prediction: The first application to the estimation of aboveground biomass," *Forests*, vol. 12, no. 2, 2021, Art. no. 216.
[57] Y. Sun, X. Jin, T. Pukkala, and F. Li, "Predicting individual tree diameter of larch (Larix olgensis) from UAV-LiDAR data using six different algorithms," *Remote Sens.*, vol. 14, no. 5, 2022, Art. no. 1125.
[58] A. Kahriman, A. Şahin, T. Sönmez, and M. Yavuz, "A novel approach to selecting a competition index: The effect of competition on individual-tree diameter growth of Calabrian pine," *Can. J. Forest Res.*, vol. 48, no. 10, pp. 1217–1226, 2018.
[59] C. Kuehne, A. R. Weiskittel, and J. Waskiewicz, "Comparing performance of contrasting distance-independent and distance-dependent competition metrics in predicting individual tree diameter increment and survival within structurally-heterogeneous, mixed-species forests of Northeastern United States," *Forest Ecol. Manage.*, vol. 433, pp. 205–216, 2019.
[60] M. Zhou, X. Lei, J. Lu, W. Gao, and H. Zhang, "Comparisons of competitor selection approaches for spatially explicit competition indices of natural spruce-fir-broadleaf mixed forests," *Eur. J. Forest Res.*, vol. 141, no. 1, pp. 177–211, 2022.
[61] J. Bergstra and Y. Bengio, "Random search for hyper-parameter optimization," *J. Mach. Learn. Res.*, vol. 13, no. 10, pp. 281–305, 2012.
[62] L. Tang, C. Chen, H. Huang, and D. Lin, "An integrated system for 3D tree modeling and growth simulation," *Environ. Earth Sci.*, vol. 74, pp. 7015–7028, 2015.

Linlong Wang (Student Member, IEEE) received the B.E. degree in forestry from Huazhong Agricultural University, Wuhan, China, in 2012, and the M.E. degree in ecology in 2015 from Chinese Academy of Forestry, Beijing, China, where he is currently working toward the Ph.D. degree in forestry information technology.

His research interests include deep learning and and 3-D forest visualization.

Huaiqing Zhang (Senior Member, IEEE) received the B.S. degree from Central South Forestry College, Changsha, China, in 1996, and the Ph.D. degree in forest management from the Chinese Academy of Forestry, Beijing, China, in 2001.

From 2001 to 2023, he was with the Institute of Resource Information, Chinese Academy of Forestry, where he has been a Researcher since 2010. His research interests include forestry information technology, virtual reality, artificial intelligence, and 3-D visualization.

Kexin Lei (Student Member, IEEE) received the B.S. degree in geographic information science from Guizhou Normal University, Guiyang, China, in 2021. Since 2021, she has been working toward the Ph.D. degree in forestry information technology with the Institute of Resource Information, Chinese Academy of Forestry, Beijing, China.

Her research interests include forestry information technology, virtual reality, and artificial intelligence.

Tingdong Yang received the B.E. degree in information engineering from the Henan University of Science and Technology, Luoyang, China, in 2013, and the M.S. degree in forestry information engineering from Central South University of Forestry and Technology, Changsha, China, in 2016.

From 2016 to 2023, he was with the Institute of Forest Resource Information Techniques, Chinese Academy of Forestry, Beijing, where he has been an Assistant Professor since 2018. His research interests include forestry 3-D visual simulation technology.

Jing Zhang received the B.E. degree in hydrology and water resources engineering from Heilongjiang University, Harbin, China, in 2017 and the M.S. degree in forest management from Nanjing Forestry University in 2020.

Since 2020, he has been with the Institute of Forest Resource Information Techniques, Chinese Academy of Forestry, mainly focusing on artificial intelligence, remote sensing, and geographic information system.

Zeyu Cui Zeyu Cui (Student Member, IEEE) received the M.S. degrees in forestry in 2022 from the Chinese Academy of Forestry (CAF), Beijing, China, where he is currently working toward the Ph.D. degree in forestry information technology with the Institute of Forest Resource Information Techniques.

His research interests include forestry artificial intelligence and visual simulation research.

Rurao Fu (Student Member, IEEE) received the B.S. degree in forestry from JiangXi Agricultural University, Nanchang, China, in 2023. Since 2023, he has been working toward the master's degree with the Chinese Academy of Forestry, Beijing, China.

His research interests include forestry, forest management, artificial intelligence, and 3-D visualization.

Hongyan Yu received the B.S. degree in plant protection from Northwest A&F University (NWAFU), Xianyang, China, in 2001, and the M.E. degree in ecology from Qinghai University, Xining, China, in 2007.

Her research focuses on grassland ecological protection.

Baowei Zhao received the B.S. degree in forestry from Northwest A&F University (NWAFU), Xianyang, China, in 2018.

His research interests include intelligent forest and grass ecological protection.

Xianyin Wang received the B.S. degree in spatial information and digital technology from the Xiamen University of Technology (XMUT), Xiamen, China, in 2019.

Her research interests include intelligent forest and grass ecological protection.